We are IntechOpen,
the world's leading publisher of
Open Access books
Built by scientists, for scientists

4,800
Open access books available

122,000
International authors and editors

135M
Downloads

Our authors are among the

154
Countries delivered to

TOP 1%
most cited scientists

12.2%
Contributors from top 500 universities

CLARIVATE ANALYTICS
BOOK CITATION INDEX
INDEXED

WEB OF SCIENCE™

Selection of our books indexed in the Book Citation Index
in Web of Science™ Core Collection (BKCI)

Interested in publishing with us?
Contact book.department@intechopen.com

Numbers displayed above are based on latest data collected.
For more information visit www.intechopen.com

An Idealised Biphasic Poroelastic Finite Element Model of a Tibial Fracture

Sanjay Mishra

School of Engineering Systems, Queensland University of Technology, Brisbane,
Australia

1. Introduction

The outcome of a bone fracture partly depends upon the mechanical environment experienced by the fracture callus (reparative tissue) during the healing. Therefore biomechanics of bone fracture healing has been examined in many clinical or biological, mathematical or finite element studies (Cheal et al. 1991, DiGioia et al. 1986, Claes et al. 1999, Doblaré et al. 2004 and Oh et al. 2010). Most of the studies model the components of bone fractures as monophasic, homogenous materials, which may not be appropriate considering the large inter fragmentary displacements and high porosity of the reparative tissue. Therefore, this study describes an idealised mathematical model of a healing bone fracture with biphasic approach when the callus bone is modelled as mixture of solids and fluids.

Markel *et al.* (1990) reported that the porosity of the callus in a healing canine osteotomy decreased from 99.6% at 2 weeks to 38% at 12 weeks. Therefore, the biphasic, poroelastic model for fracture callus and bone has been suggested in the literature (Carter *et al.* 1998, Simon *et al.* 1992, Prendergast et al1997, Spilker *et al.* 1990). Biphasic poroelastic models for soft tissues (Mow *et al.* 1980, Simon *et al.* 1985, Van Driel *et al.* 1998, Prendergast *et al.* 1997, Spilker *et al.* 1990) have been developed and applied to model cartilage (Mow *et al.* 1980) and intervertebral discs (Simon *et al.* 1985). Van Driel *et al.* (1998) and Prendergast *et al.* (1997) modelled tissue adjacent to prostheses using poroelastic material properties to investigate tissue differentiation. In the field of fracture healing however, only monophasic material properties of callus have been simulated (Carter 1988, Carter 1998, Blenman 1989, Cheal 1991, DiGioia 1986, Claes 1999, Gardner 1998 and 2000). This is probably because of the paucity of data in the literature on the values of parameters required to define the biphasic material properties of fracture callus. Simulation of a biphasic, compressible, anisotropic, linear poroelastic material model requires forty material constants (Simon 1992). Even the very simplified simulation of an isotropic material requires a minimum of five material constants. However, the number of material constants required to simulate a biphasic, poroelastic medium can be further reduced to three if the solid and fluid media are assumed to be incompressible (Simon 1992). These three independent material parameters are Lame's material stiffness parameters (λ and μ) and hydraulic permeability (k). Alternatively, Zienkiewicz and Taylor (1994b) suggested a method to model poroelastic behaviour under `undrained' condition using the modulus of elasticity, Poisson's ratio, the

porosity of the matrix, and the bulk modulus of the fluid phase. In the present study, a finite element model (FEM) based on the poroelastic behaviour of the `undrained' callus at four temporal stages of healing is developed by modifying the theory proposed by Zienkiewicz and Taylor (1994). This model was developed to examine the influence of fluid pressure on the pattern of healing and to compare the distribution of stresses in the callus with the monophasic solutions developed for the same subject at the same temporal points reported earlier by Gardner *et al.* (2000).

2. Materials and methods

2D, monophasic, plane stress, FEM's of a mid-diaphyseal tibial fracture were developed at four stages during healing (4, 8, 12, and 16 weeks post operation) by Gardner *et al.* (2000). The geometry and the regionalisation of the callus are shown in Figure 1. The geometry, finite element meshing, boundary conditions (Figure 2) and applied displacements (Table 1) used in the study of Gardner *et al.* (2000) are adopted in the biphasic poroelastic models of the present study. The tissue histology and calculated elastic moduli of regions of callus at four stages of healing are shown in Table 2.

Week	x(mm)	y(mm)	Z(radians)
4	.283	-.377	-.00329
8	-.015	-.159	.00201
12	-.092	-.260	.00169
16	-.129	-.111	-.00215

Table 1. Interfragmentary displacements measured during walking corresponding to peak longitudinal displacements. y (longitudinal), x (transverse), Z (rotational in x-y plane) adopted from the study of Gardner *et al.* (*2000*).

Stage	CENTRAL		ADJACENT		PERIPHERAL	
weeks	tissue type	Modulus (MPa)	tissue type	Modulus (MPa)	tissue type	Modulus (MPa)
4	Haematoma, granulated tissue	0.9	Soft connective tissue with invading vasculature	3.8	Soft fibrocartilage tissue	76
8	Fibrous perichondrial tissue	28	Woven bone, 25% maturation	700	Dense fibrous tissue, 45% maturation	2800
12	Fibrous perichondrial tissue	30.6	Woven bone, 25% maturation	765	Dense fibrous tissue, 45% maturation	3060
16	Fibrous cartilage tissue, 10% maturation	75	Woven bone, 60% maturation	5000	Bone, 100% maturation	20000

Table 2. Tissue histology and calculated Young's moduli of the three regions of fracture callus, at 4, 8, 12 and 16 weeks post fracture adopted from the study of Gardner *et al.* (2000).
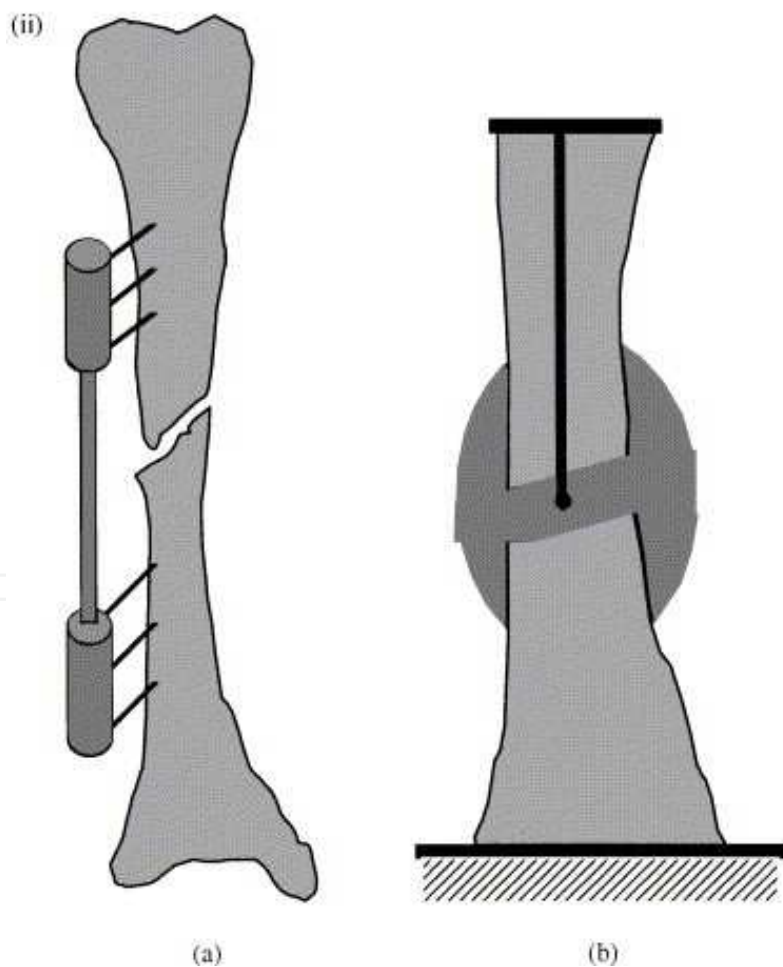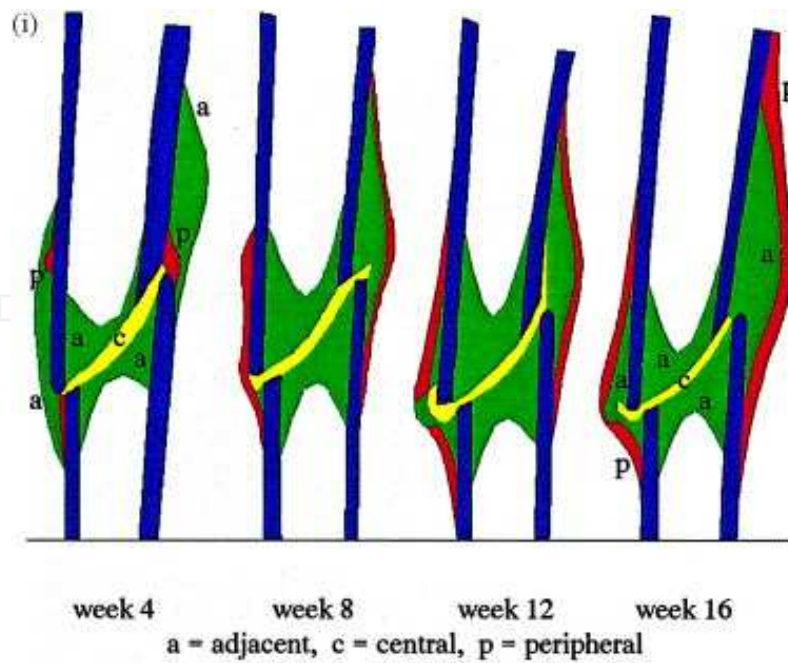
Fig. 1. (i) Regions of cortical bone and callus in the 2D finite element models a- adjacent (green), c- central (yellow), p- peripheral (red), (ii) Schematic diagram showing the bone fracture, external fixation device and callus region (adopted from Gardner *et al. (2000*).
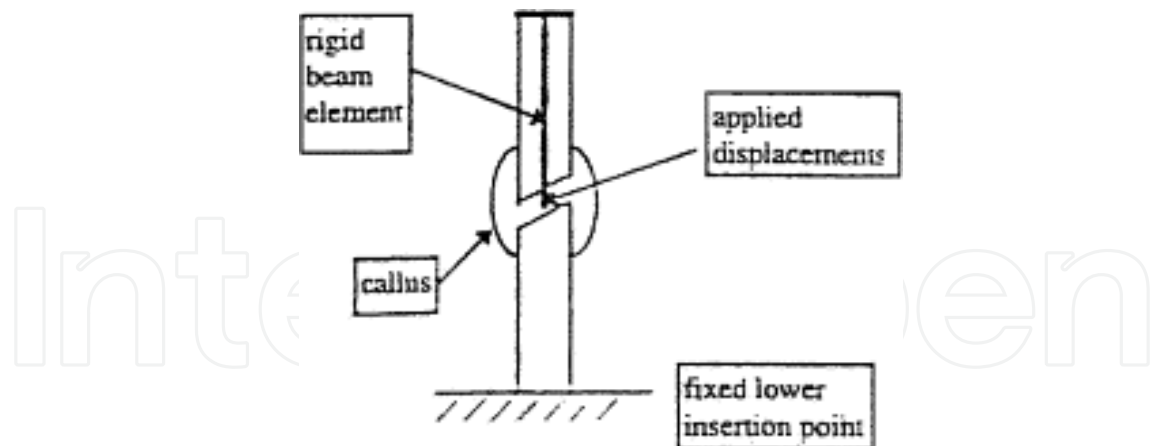
Fig. 2. Boundary condition of the finite element model, showing the fixed lower boundary and the displacement of the upper bone fragment applied at the fracture centre adopted from the Gardner *et al.* (*2000*).

However, the callus tissue in the present study was idealised as a homogenous, fully saturated, linear poroelastic medium consisting of a matrix of solid and incompressible fluid, as opposed to the monophasic material properties in the study of Gardner *et al.* (2000). The following section describes the theory employed for calculating equivalent poroelastic material properties of the callus from the modulus of elasticity, Poisson's ratio, porosity and bulk modulus of the fluid of the callus tissue. Unlike a monophasic medium, the normal stress acting across a plane within a biphasic poroelastic mass will have two components, an inter-granular pressure known as effective pressure or effective stress, and a fluid pressure called the pore pressure. The sum of these two will constitute the total normal stress. The volume change characteristics and the strength of poroelastic mediums are controlled by the effective stress not by the total stress. Thus the only difference between the present study and the previous study of Gardner et al. (2000) is that the constitutive equation of the callus is changed from monophasic medium to a biphasic poroelastic medium.

3. Mathematical description of the model

For 2D plane stress analysis, the constitutive equation for a monophasic material (Zienkiewicz and Taylor (1994a)) is

$$\boldsymbol{\sigma} = \begin{Bmatrix} \sigma_x \\ \sigma_y \\ \tau_{xy} \end{Bmatrix} = \mathbf{D} \begin{Bmatrix} \varepsilon_x \\ \varepsilon_y \\ \gamma_{xy} \end{Bmatrix} \tag{1}$$

Where $\boldsymbol{\sigma}$ is total stress. σ_x , σ_y are normal stresses in the *x* and *y* directions, τ_{xy} is shear stress in the *x-y* plane, ε_x , ε_y are normal strains in the *x* and *y* directions and γ_{xy} is the shear strain in the *x-y* plane. For plane stress analysis the constitutive matrix $\mathbf{D}$ (Zienkiewicz and Taylor 1994a) is defined as

$$\mathbf{D} = \frac{E}{1-v^2} \begin{bmatrix} 1 & v & 0 \\ v & 1 & 0 \\ 0 & 0 & \dfrac{1-v}{2} \end{bmatrix} \tag{2}$$

Where E and v are the Young's Modulus and the Poisson's ratio of the material.

A plane stress, linear elastic finite element program can be used to analyses the linear elastic plane strain problem (Zienkiewicz and Taylor (1994a)) by substituting

$$E = E_s = \frac{E_n}{1-v_n^2} \tag{3a}$$

and

$$v = v_s = \frac{v_n}{1-v_n} \tag{3b}$$

Where subscript 's' denotes plane stress parameters and 'n' denotes plane strain parameters. Substituting equation (3a) and (3b) into equation (2), we have

$$\mathbf{D} = \frac{\dfrac{E_n}{1-v_n^2}}{1-\left(\dfrac{v_n}{1-v_n}\right)^2} \begin{bmatrix} 1 & \dfrac{v_n}{1-v_n} & 0 \\ \dfrac{v_n}{1-v_n} & 1 & 0 \\ 0 & 0 & \dfrac{1-\dfrac{v_n}{1-v_n}}{2} \end{bmatrix} \tag{4a}$$

Simplifying

$$\mathbf{D} = \frac{E_n(1-v_n)^2}{(1-2v_n)(1-v_n^2)} \begin{bmatrix} 1 & \dfrac{v_n}{1-v_n} & 0 \\ \dfrac{v_n}{1-v_n} & 1 & 0 \\ 0 & 0 & \dfrac{1-2v_n}{2(1-v_n)} \end{bmatrix} \tag{4b}$$

$$\mathbf{D} = \frac{E_n(1-v_n)}{(1-2v_n)(1+v_n)} \begin{bmatrix} 1 & \dfrac{v_n}{1-v_n} & 0 \\ \dfrac{v_n}{1-v_n} & 1 & 0 \\ 0 & 0 & \dfrac{1-2v_n}{2(1-v_n)} \end{bmatrix} \tag{4c}$$

Thus a linear elastic plane strain **D**-matrix is obtained.
The equation for static equilibrium in 2D (Dawe 1984) is:

$$(\partial \sigma_x / \partial x) + (\partial \tau_{xy} / \partial y) + R_x = 0 \tag{5a}$$

$$(\partial \sigma_y / \partial y) + (\partial \tau_{xy} / \partial x) + R_y = 0 \tag{5b}$$

Using the definition of effective stress (Zienkiewicz and Taylor (1994b))

$$\sigma_X = \sigma'_X - p \tag{6a}$$

$$\sigma_Y = \sigma'_Y - p \tag{6b}$$

$$\tau_{XY} = \tau'_{XY} \tag{6c}$$

where $\sigma_X, \sigma_Y, \tau_{XY}$ are total stresses; R_x, R_y are body forces; σ'_X, σ'_Y, τ'_{XY} are effective stresses (positive value for tensile stresses and negative for compressive stresses), p is pore pressure of the fluid, which is conventionally described as positive for compressive pressure and negative for tensile pressure.
The combined seepage and conservation of fluid equation described by Zienkiewicz and Taylor (1994b) is:

$$-\frac{\partial}{\partial x}\left(k\frac{\partial p}{\partial x}\right) - \frac{\partial}{\partial y}\left(k\frac{\partial p}{\partial y}\right) + \frac{\dot{p}}{Q} + \dot{\varepsilon}_X + \dot{\varepsilon}_Y = 0 \tag{7}$$

Where k is the permeability of the fluid, Q is the ratio of the bulk modulus of fluid to the porosity of the media and $\varepsilon_X, \varepsilon_Y$ represent the volumetric strain rates of the solid skeleton. The superscript 'dot' denotes differentiation with respect to time. Since the gait cycle frequency of this clinical fracture was approximately 1 Hz, it is reasonable to assume that little or no seepage from the callus occurs during loading (Carter 1998, Gardner 1998). Therefore, because the time scale is short, if the local `undrained' condition of the callus is assumed, permeability 'k' can also be assumed to be effectively zero. Under these conditions, Equation 7 becomes:

$$\frac{\dot{p}}{Q} + \dot{\varepsilon}_X + \dot{\varepsilon}_Y = 0 \tag{8}$$

Or

$$\dot{p} = -Q(\dot{\varepsilon}_X + \dot{\varepsilon}_Y) \tag{9}$$

Integrating with respect to time and assuming homogenous initial conditions ($p = 0$, $\varepsilon_X = \varepsilon_Y = 0$ at $t = 0$):

$$p = -Q(\varepsilon_X + \varepsilon_Y) \tag{10}$$

Substituting this value in equation (6a) and (6b) gives:

$$\sigma_{xx} = \sigma'_{xx} + Q(\varepsilon_X + \varepsilon_Y) \tag{11}$$

$$\sigma_{yy} = \sigma'_{yy} + Q(\varepsilon_X + \varepsilon_Y) \tag{12}$$

Expanding for two-dimensional plane strain analysis ($\sigma_z \neq 0$) gives:

$$\begin{Bmatrix} \sigma_x \\ \sigma_y \\ \sigma_z \\ \tau_{xy} \end{Bmatrix} = \begin{Bmatrix} \sigma_x^{'} \\ \sigma_y^{'} \\ \sigma_z^{'} \\ \tau_{xy}^{`} \end{Bmatrix} + Q \begin{Bmatrix} \varepsilon_x + \varepsilon_y + \varepsilon_z \\ \varepsilon_x + \varepsilon_y + \varepsilon_z \\ \varepsilon_x + \varepsilon_y + \varepsilon_z \\ 0 \end{Bmatrix} \qquad (13)$$

Noting that the material behaviour is controlled by the effective stress in a poroelastic medium, then

$$\boldsymbol{\sigma}' = \mathbf{D}\boldsymbol{\varepsilon} \qquad (14)$$

Combining equation (13) and (14):

$$\begin{Bmatrix} \sigma_x \\ \sigma_y \\ \sigma_z \\ \tau_{xy} \end{Bmatrix} = \mathbf{D} \begin{Bmatrix} \varepsilon_x \\ \varepsilon_y \\ \varepsilon_z \\ \gamma_{xy} \end{Bmatrix} + \begin{bmatrix} Q & Q & Q & 0 \\ Q & Q & Q & 0 \\ Q & Q & Q & 0 \\ 0 & 0 & 0 & 0 \end{bmatrix} \begin{Bmatrix} \varepsilon_x \\ \varepsilon_y \\ \varepsilon_z \\ \gamma_{xy} \end{Bmatrix} \qquad (15)$$

If the modified stress-strain relationship is defined as:

$$\boldsymbol{\sigma} = \mathbf{D'}\boldsymbol{\varepsilon} \qquad (16)$$

then

$$\mathbf{D}' = \begin{bmatrix} D_{11}+Q & D_{12}+Q & D_{13}+Q & 0 \\ D_{21}+Q & D_{22}+Q & D_{23}+Q & 0 \\ D_{31}+Q & D_{32}+Q & D_{33}+Q & 0 \\ 0 & 0 & 0 & D_{44} \end{bmatrix} \begin{Bmatrix} \varepsilon_x \\ \varepsilon_y \\ \varepsilon_z \\ \gamma_{xy} \end{Bmatrix} \qquad (17)$$

and

$$Q = K_f / n, \qquad (18)$$

where K_f is the bulk modulus of the fluid phase and n is the porosity of the porous media. Thus the $\mathbf{D'}$ matrix (Equation 17) for a poroelastic medium can be calculated by substituting Q values in the $\mathbf{D}$ matrix of corresponding plane strain analysis (Equation 4C). The $\mathbf{D}$ matrix can be expanded to calculate the new set of material properties, E and v, corresponding to the poroelastic material behaviour under undrained condition.

4. Development of the poroelastic FEM from the monophasic FEM

Using the above theory, a new set of material properties (E and v) were calculated from the refined values of E and v of the monophasic model of Gardner *et al.* (2000) and the values of Q described in this section. At first, the proportion of calcified tissue in the callus was extrapolated from data (at $E = 800$ MPa 20% calcification; at $E = 2000$ MPa 40% calcification;

at *E* = 8000 MPa 70% calcification and at *E* = 18000 MPa 100% calcification occurs) taken from Davy and Connoly (1982) for the new bone at intermediate densities corresponding to the elastic moduli of the callus adopted from the study of Gardner *et al.* (*2000*). The calculated calcification of the different regions of callus at 4, 8, 12 and 16 weeks is shown in Table 3. The porosity of the callus tissue was then assumed to be inversely related to the proportion of the calcified tissue present in the callus (Carter 1977), and therefore was found to vary from 0.9 for soft callus (<5% calcification) to 0.3 for woven bone (100% calcification). As the porosity of 0.8 was used by Van Driel *et al.* (1998) for soft fibrous, cartilage and bone tissues, by comparison 0.9 appeared valid for the softer tissues of the present model. The porosity of 0.3 was suggested for woven bone (Carter 1977) which seems to be valid for the harder tissues of the present model. All intermediate values of porosities were linearly extrapolated from these two values at corresponding values of calcification shown in Table 3. The interstitial fluid in the callus was assumed to have the bulk modulus (K_f) of salt water (2.3 GPa) (Cowin 1999).

Time weeks	Callus	E_m (MPa)	v_m	Calcification %	n	Q (K_f/n)	E_p (MPa)	v_p
4	central	0.9	0.39	<5	0.9	2555	0.2	0.499
	adjacent	3.8	0.39	<5	0.9	2555	4.38	0.499
	Peripheral	76	0.39	8.8	0.88	2643	81	0.494
8	central	28	0.39	5	0.89	2613	30	0.498
	adjacent	700	0.30	24	0.78	2948	786	0.46
	Peripheral	2800	0.30	44	0.64	3593	3023	0.43
12	central	30.6	0.39	5	0.89	2613	33	0.497
	adjacent	765	0.30	25	0.78	2948	858	0.457
	Peripheral	3060	0.30	46	0.64	3593	3291	0.398
16	central	75	0.30	8.8	0.88	2643	86	0.494
	adjacent	5000	0.30	57	0.57	4035	5283	0.373
	Peripheral	20000	0.30	100	0.3	7666	20381	0.324

Table 3. Calculation of the equivalent poroelastic material properties of the callus from the monophasic material properties.Note: subscript 'm' denotes the monophasic model and 'p' denotes the biphasic poroelastic model. K_f = 2.3 GPa (Cowin 1999).

5. Results

Figures 3 and 4 show the contour diagrams of the fluid pressure, effective stress and total stress in the callus at 4, 8, 12 and 16 weeks post fracture. Additional figures of effective stresses showing only one region of the callus were also drawn for clarity and the results are shown in Table 4. At Week 4 (Figure 3a) the peak compressive fluid pressures (≥ 400 MPa) were present in the cortical gap region, intermediate pressures (≥ 150 MPa) were present in the other regions of the interfragmentary gap and the periosteal regions close to the interfragmentary gap, and low pressures (≤ 50 MPa) were present in the regions of the callus remote to the interfragmentary gap. Tensile pressures of up to 100 MPa were present

in localised regions of the endosteal callus. At Week 8 [Figure 3(d)] fluid pressures in all regions of the callus were reduced (< ± 5 MPa) but elevated pressures (>70 MPa) were present in the cortical gap regions. At Week 12 [Figure 4(a)], fluid pressures of greater than 100 MPa are seen medially and less than 25 MPa laterally in the cortical gap region. All other regions indicated low pressures (<10 MPa); however, tensile pressures of about 30 MPa are indicated in the subperiosteal region on the lateral side. At Week 16 [Figure 4 (d)], fluid pressures are further reduced in all regions of the callus, although in the medial inter-cortical gap they remained elevated (15 < P < 25 MPa). Inter cortical fluid pressures are reduced laterally almost to the level of the periosteal callus (0 < P < 1 MPa).
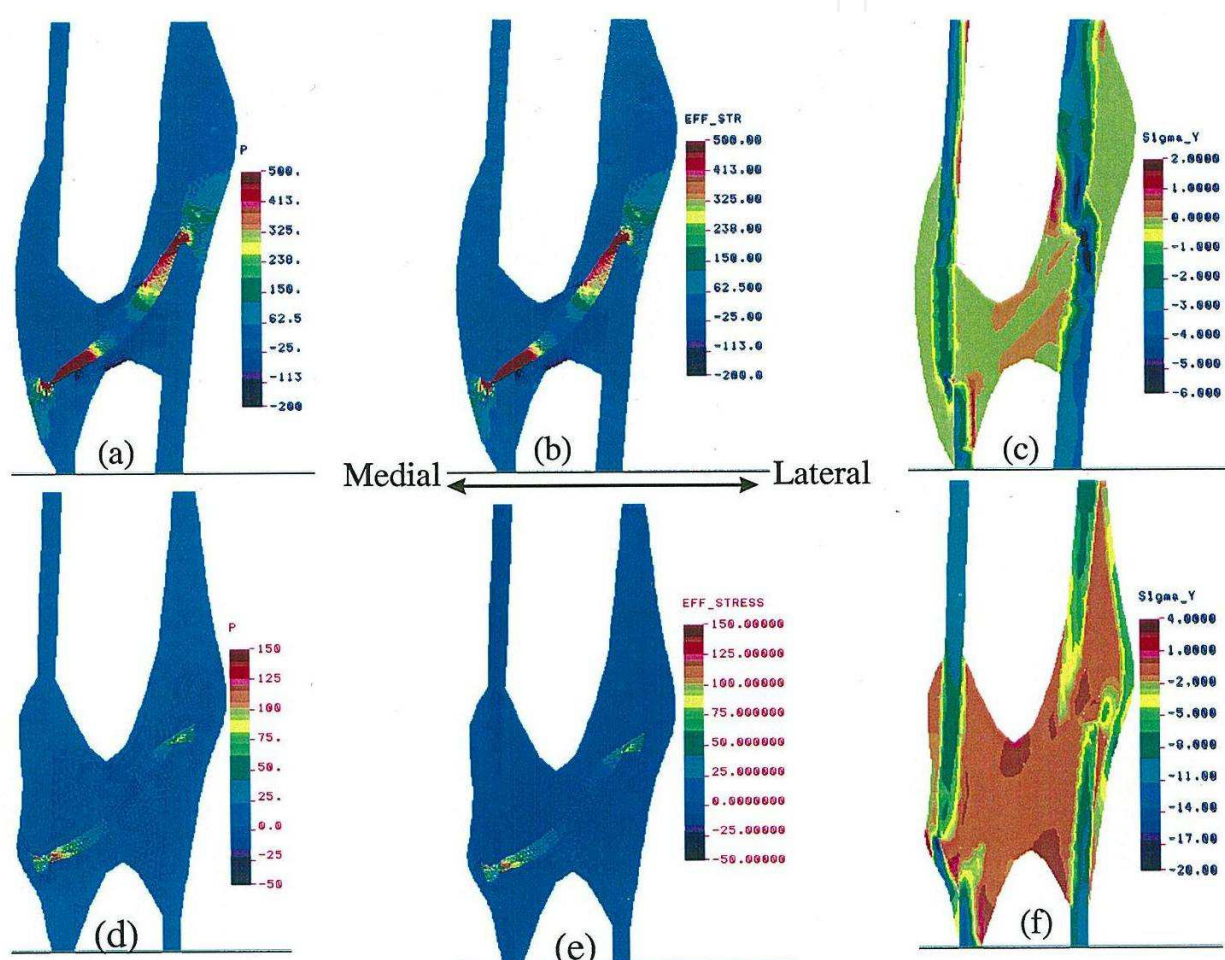
Fig. 3. Fluid pressure (p), effective stress (EFF_STR) and total stress (Sigma_Y) in the callus at 4 weeks [(a), (b) and (c)] and at 8 weeks [(d), (e) and (f)].

Effective stress diagrams are similar in magnitude and distribution to the fluid pressure diagrams. As expected, the total stresses (σ_Y) were very low as compared to the corresponding fluid pressures (p) because during undrained loading condition, most of the load is taken by fluid medium. Also, in the regions of low fluid pressures the effective stress magnitudes (Table 4) are approximately equal to the total stresses. The total pressure diagrams [Figures 3 and 4 (c) (f)] are similar to the corresponding longitudinal stress diagrams of the monophasic model reported earlier by Gardner *et al.* (*2000*).
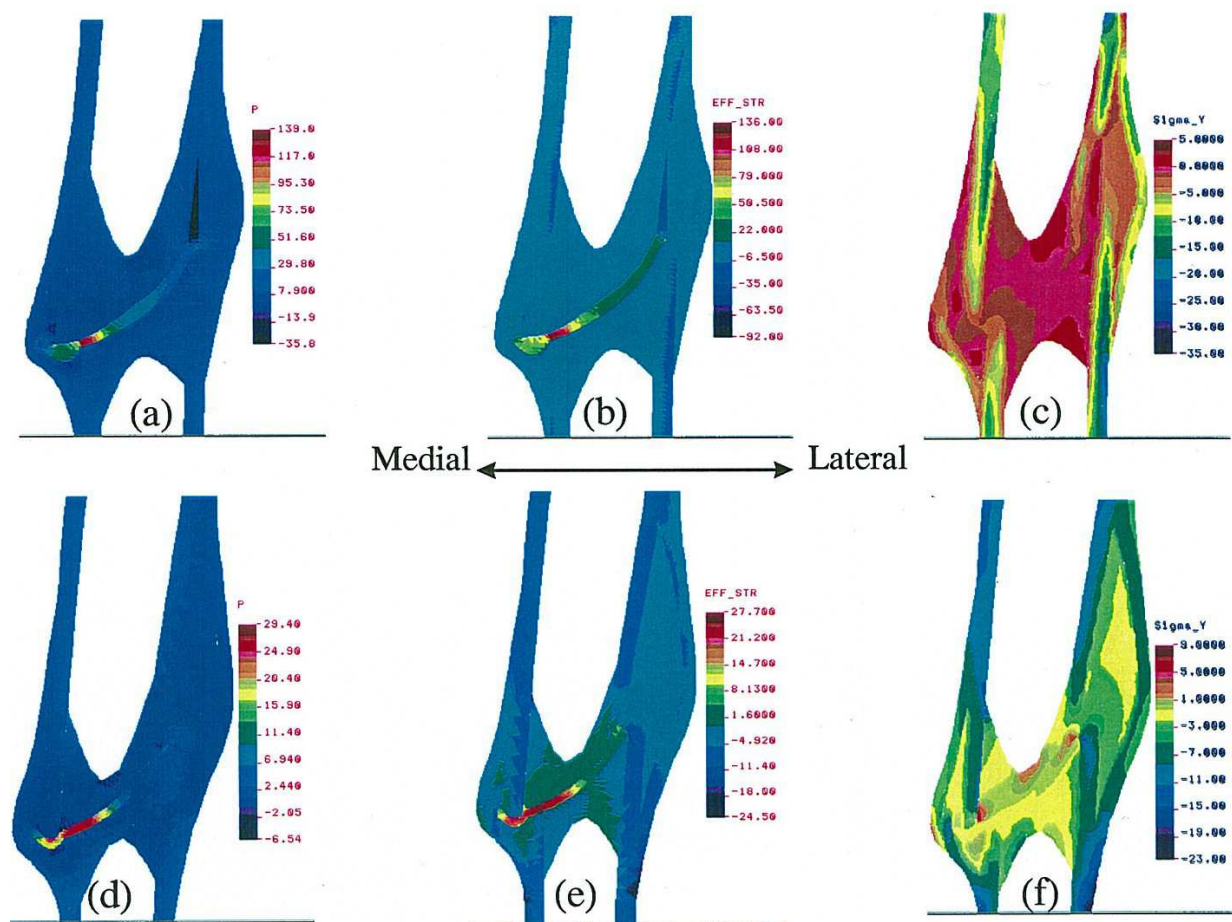
Fig. 4. Fluid pressure (p), effective stress (EFF_STR) and total stress (Sigma_Y) in the callus at 12 weeks [(a), (b) and (c)] and at 16 weeks [(d), (e) and (f)].

Time in Weeks	Callus region	Monophasic model Longitudinal stress (MPa)	Biphasic model Effective stress (MPa)
4	Central	-1.5 to 0.5	100 to 1000
	Adjacent	-1.5 to 0.5	100 to 500
	Peripheral	-1.5 to 0.5	25 to 500
8	Central	-1 to 2	25 to 150
	Adjacent	-5 to 2	-1 to 1
	Peripheral	-15 to -1	-1 to 1
12	Central	-3 to 1	100 to 500
	Adjacent	-8 to 1	25 to 50
	Peripheral	-3 to -15	0 to 12
16	Central	0 to 4	100 to 150
	Adjacent	-3 to 0	-1 to 1
	Peripheral	-3 to -11	-1 to -5

Table 4. Longitudinal stress ranges in the monophasic model of Gardner *et al.* (*2000*) and effective stress ranges in the biphasic poroelastic model.

6. Discussion and conclusions

The magnitudes of fluid pressure and effective stress are very high and therefore appear unrealistic. In particular, the high tensile stress would produce cavitation or may lead to gas in the pore fluid, and the callus matrix may be ruptured. These conditions are typical of the undrained simulation behaviour under large deformations. In reality, no matter how small the permeability of the poroelastic medium or how rapid is the loading, fluid flow will occur under such high-pressure gradient. Therefore the absolute value of pressure and the presence of high tensile pressure in the callus are more an artifact of the modelling technique than are the patterns of the distribution of pressure and their trend in variation. Thus, for this technique of modelling the presence of spatial or temporal pressure gradients within the callus may be a valid indicator of the flow of fluid in the form of blood, nutrients or waste products. For example, the tensile fluid pressure regions of the present models at peak loading during walking are likely to show reduced magnitudes of tensile pressure or compressive pressure during unload phases. The hydraulic gradient will be reversed and the fluid flow will be in the opposite direction. This alternate inflow and outflow of fluid may be related to the transport mechanism of inflow of nutrients and oxygen, and outflow of waste products and carbon dioxide from the callus. Such inflow and outflow may enhance the growth of capillary blood vessels, thus accelerating the healing process.

It can be envisaged from the above that if the movement is too small, the change in fluid pressure will be small and the beneficial effect will also be small. Therefore the results of the present study corroborate those of other studies (Kenwright 1998, Sarmiento and Latta 1995, Goodship and Kenwright 1985, Kenwright and Goodship 1989) suggesting that fracture site movement is necessary for efficient secondary healing. However, if the movement is too large the fabric of the callus matrix could be damaged because of the cyclical expansion and compression, and this damage could hinder healing.

Furthermore, if the frequency of the movement were too high, the time interval between pressure gradient reversals would be too small for the fluid to flow. On the other hand, if the frequency is too low, fluid will penetrate the tissues before any substantial hydraulic gradient can be developed. Since the present study was limited to a single temporal point during the gait cycle it is not possible to define the optimum magnitude and frequency of movement beneficial for healing. Models that simulate the different temporal points of the gait cycle may provide more information about the optimum movements for fracture patients.

At Week 4 (Figure 3a), there are high compressive fluid pressures in the inter fragmentary gap regions because the undrained model is under large compressive displacement and fluid is unable to flow out side the system boundary. In this condition the loads is predominantly taken by an incompressible fluid that controls the motion of the bone fragments and provides support for intact tissues. It does this by increasing the stiffness of the limb and it also protects the fracture from further damage (Sarmiento and Latta 1995). Since fluid pressure is a function of movement, the cortical gap locations are expected to undergo higher pressures than locations further away from the gap, as shown in Figure 3a. It is worth noting that at this stage the callus is comprised of more than 90% fluid, therefore the incompressible fluid will resist high pore pressure.

At Week 8, reduction in the porosity (Table 3) and compressive interfragmentary displacement (Table 1) of the callus reduce fluid pressure. However, at Week 12, the porosity remains almost constant (Table 3) compared to Week 8 but the applied compressive interfragmentary

displacement increases (Table 1), resulting in elevated fluid pressures in the adjacent callus. At Week 16, both the applied compressive interfragmentary displacement and the fluid pressure in the callus reduce. Therefore fluid pressures appear to be more sensitive to longitudinal interfragmentary displacements than to the callus-porosity in the present study.

Fluid pressure distribution patterns correlate with the general pattern of ossification, as reported by others (Blenman 1989,Carter 1988, Sarmiento 1995, Yamagishi 1955). Blenman and Carter (1989) suggested that ossification progresses through the stages of `bone tuft', `bone wedge' and `bone bridge' and poroelastic models appear to corroborate this if it is believed that ossification may not take place in the regions of high fluid pressures. At Week 4, high pore pressure regions of the interfragmentary gap divide the proximal and distal callus. Therefore it appears that ossification is possible only in the low-pressure regions of the periosteal callus away from the interfragmentary gap, forming the `wedge' shaped ossified callus. At Weeks 8 and 12, fluid pressure in the callus is reduced almost to zero at the level of the gap, thus allowing the formation of a `bridge' of ossified callus between the `wedges'. Since the present study started at 4 weeks post operation, a pattern similar to that of the `tufts' theory may have also been present before this stage.

The similarity between the magnitude and pattern of total stress diagrams of the biphasic poroelastic model and the corresponding longitudinal stress diagrams of the monophasic model of Gardner *et al.* (2000) are expected. This is because total stress is a function of the total force and total cross section area (Wood 1990) of the callus, which remain similar in both the models.

The greatest disparities between the monophasic and biphasic solutions occur in initial healing at Week 4. This disparity exists because the soft callus has a high porosity initially and is subjected to high tensile stresses during the large applied initial displacements. As the callus calcifies, its porosity and the fluid pressures decrease so that total stress is closer to the effective stress. This effect of porosity is evident from Table 4, where the maximum difference between stresses from the two models is in the high-porosity central callus and the minimum difference is in the low-porosity peripheral callus. The patterns of effective stress in the biphasic models also differ from the corresponding monophasic models. In the biphasic models, substantial variations of stress are evident at the cortical gap, sub periosteal and endosteal callus. Whereas in general, the monophasic models reported by Gardner *et al.* (2000) predicts similar stress regimes throughout the central and adjacent callus. Therefore, if the differentiation and maturation of the callus are believed to be influenced by the preceding stress environments, then the biphasic models appear to predict more realistic patterns of tissue differentiation and maturation.

7. Limitations of the study

The results of the present study should be evaluated under modelling limitations. Firstly, solutions are valid only for the `undrained' condition that assumes that no fluid moves out of the system boundary during loading, but in reality a small amount of fluid may drain through the pores of the callus. However this drainage may not have invalidated the results of the present study as the gait cycle frequency is approximately 1 Hz, and physiological loading periods during the stance phase of gait are around 0.3 to 0.5 seconds, which is probably too rapid for significant drainage of fluid to take place (Gardner et al. 1998, *2000*). Secondly, the callus has been idealised as a linear, elastic, fully-saturated porous medium throughout healing. These idealised conditions may also be responsible for the high magnitudes of fluid

pressure, whereas actual pressures are believed to be lower than predicted by the present model. However, the pattern and trend of temporal variations in fluid pressures during progressive ossification are unlikely to change significantly as a result of applying slightly different poroelastic material properties and constitutive equations.

Despite the limitations of the present model, these results indicate that the biphasic material properties of the callus are more appropriate to the initial soft callus stage of healing and support the suggestion of Sarmiento and Latta (1995) "The incompressible fluid effect, or hydraulics is most important in early post injury period. We feel that hydraulics is responsible for the control of motion of fragments before callus has developed and that it provides the significant degree of stiffness observed in loaded limbs with fresh fractures fit with fracture braces."

8. Acknowledgement

9. References

Blenman, P. R., Carter, D. R., and Beaupre, G. S. (1989) Role of mechanical loading in the progressive ossification of a fracture callus. *J. Orthop. Res.* 7, 398-407.

Carter D, Hayes WC. (1977) The compressive behaviour of bone as a two phase porous structure. JBJS,59A (7):954-962

Carter D. R., Blenman P. R., and Beaupre G. S. (1988) Correlations between mechanical stress history and tissue differentiation in initial fracture healing. *J. Orthop. Res.* 6, 736-748.

Carter D. R., Beaupre G.S., Giori N.J., and Helms J.A. (1998) Mechanobiology of skeletal regeneration. Clin. Orthp. Rel. Res., 355 S: 41-55

Carter D. R., Blenman P. R., and Beaupre G. S. (1988) Correlations between mechanical stress history and tissue differentiation in initial fracture healing. *J. Orthop. Res.* 6, 736-748.

Dawe D.J., (1984) Matrix and finite element displacement analysis of structures. Clarendon press, Oxford (UK).

Doblaré M , García J.M., and Gómez J.M., (2004). Modelling bone tissue fracture and healing: a review; Engineering Fracture Mechanics, 71(13-14),1809-1840.

Cheal E. J., Mansmann K. A., DiGioia III A. M., Hayes W. C. and Perren S. M. (1991) Role of interfragmentary strain in fracture healing: ovine model of a healing osteotomy. *J. Orthop. Res.* 9:1, 131-142.

Claes, L. E., Heigele, C. A., (1999) Magnitudes of local stress and strain along bony surfaces predict the course and type of fracture healing.J. Biomech.32:3, 255-265.

Cowin S.C. (1999) Bone poroelasticity. J Biomech, 32:217-238.

Davy, D. T. and Connolly, J. F. (1982) The biomechanical behaviour of healing canine radii and ribs. *J. of Biomech.* 15:4, 235-247.

DiGioia III, A. M., Cheal, E. J., and Hayes, W. C. (1986) Three-dimensional strain fields in a uniform osteotomy gap. *J. Biomech. Eng.* 108, 273-280.

Gardner T. N, Stoll, T, Marks, L, Knothe-Tate, M. (1998) Mathematical modelling of stress and strain in bone fracture repair tissue. *Computer Methods in Biomechanics and Biomedical Engineering* Ed. by J. Middleton and GN Pandy, *Gordon and Breach Science Publishers.* 2, 247 - 254.

Gardner T.N., Marks L., Stoll T., Mishra S., Knothe Tate M., Simpson H.(2000), The influence of mechanical stimulus on the pattern of tissue differentiation in a long bone fracture - An FEM study. J. Biomechanics.33:415-25.

Kenwright, J., and Goodship, A. E. (1989) Controlled mechanical stimulation in the treatment of tibial fractures. *Clin. Orth. Rel. Res.* 241, 36-47.

Kenwright, J. and Gardner, T.N. (1998). Mechanical influences on tibial fracture healing. *Clinical Orthopaedics and Related Research.* 355S, 179-190.

Markel, M. D, Wilkenheiser, M. A. and Chao, E. Y. S. (1990) A study of fracture callus material properties: Relationship to the torsional strength of bone. *J. Orthop. Res.*, 8:6, 843-850.

Mow VC, Kuei SC, Lai WM, Armstrong C. Biphasic creep and stress relaxation of articular cartilage in compression: theory and experiments. J Biomech Engg;1980. 102:73-84.

Oh Jong-Keon, Sahu D, Yoon-Ho Ahn, et al. (2010). Effect of fracture gap on stability of compression plate fixation: A finite element study. J Orthop. Res. 28 (4): 462–467.

Prendergast, P. J., Huiskes, R. and Soballe, K. (1997) Biophysical stimuli on cells during tissue differentiation at implant interfaces. *J. of Biomech.* 30:6, 539–548.

Sarmiento, A. and Latta, l. l. (1995) Functional Fracture Bracing. Tibia, Humerus and Ulna. Springer-Verlag, Berlin.

Simon BR, Wu JSS, Carlton MW, Evans JH, Kazarian LE. Structural models for human spinal motion segments based on poroelastic view of the intervertebral disc. J Biomech Engg; 1985. 107:327-335.

Simon B. Multiphase poroelastic finite element models for soft tissue structures. Appl Mech Rev; 1992: 45(6):191-218

Simon, B. R. (1990) Poroelastic finite element models for soft tissue structures. In *Connective Tissue Matrix, Part 2* (Edited by Hukins, D.), pp. 66-90. MacMillan Press Ltd., London.

Spilker, R. L., Suh, J. K., Vermilyea, M E. and Maxian, T. A. (1990) Alternate hybrid, mixed and penalty finite formulations for the biphasic model of soft hydrated tissues. In *Biomechanics of Diarthrodial Joints* (Edited by Ratcliffe, A. and Woo, S. L-Y.), pp. 400-435. Springer, New York.

Van Driel WD, Huiskes R, Prendergast PJ. A regulatory model for tissue differentiation using poroelastic theory. In 'Poromechanics'; Ed by Thimus JF, Abousleiman Y, Cheng AHD, Coussy O, Detournay E; Publisher A A Balkema Rotterdam, The Netherlands, 1998; 409-413.

Wood D.M. (1990) Soil behaviour and critical state soil mechanics. Cambridge University Press, Cambridge (UK).

Yamagishi, M., and Yoshimura, Y. (1955) The biomechanics of fracture healing. *J. Bone Joint. Surg.* 37A, 1035-1068.

Zienkiewicz, O. C. and Bettess, P. (1982) Soils and other saturated media under transient, dynamic conditions; general formulations and the validity of various simplifying assumptions. In Soil Mechanics - *Transient and Cyclic Loads* (Edited by Pandy, G. N. and Zienkiewicz, O. C.) 1-15. John Wiley and Sons Ltd, UK.

Zienkiewicz O.C., Taylor R.L. (1994a) The Finite Element Method, Vol 1, Mcgraw Hill book Co.

Zienkiewicz O.C., Taylor R.L. (1994b) The Finite Element Method, Vol 2, Mcgraw Hill book Co.
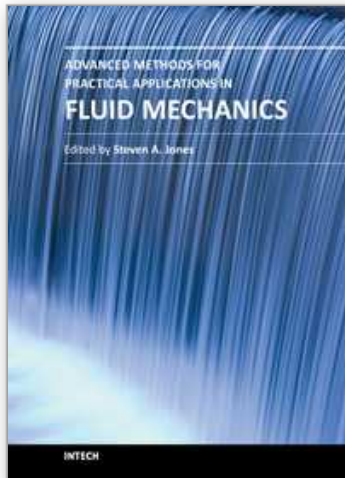
Advanced Methods for Practical Applications in Fluid Mechanics

Edited by Prof. Steven Jones

Whereas the field of Fluid Mechanics can be described as complicated, mathematically challenging, and esoteric, it is also imminently practical. It is central to a wide variety of issues that are important not only technologically, but also sociologically. This book highlights a cross-section of methods in Fluid Mechanics, each of which illustrates novel ideas of the researchers and relates to one or more issues of high interest during the early 21st century. The challenges include multiphase flows, compressibility, nonlinear dynamics, flow instability, changing solid-fluid boundaries, and fluids with solid-like properties. The applications relate problems such as weather and climate prediction, air quality, fuel efficiency, wind or wave energy harvesting, landslides, erosion, noise abatement, and health care.

How to reference

In order to correctly reference this scholarly work, feel free to copy and paste the following:

Sanjay Mishra (2012). An Idealised Biphasic Poroelastic Finite Element Model of a Tibial Fracture, Advanced Methods for Practical Applications in Fluid Mechanics, Prof. Steven Jones (Ed.), ISBN: 978-953-51-0241-0, InTech, Available from: http://www.intechopen.com/books/advanced-methods-for-practical-applications-in-fluid-mechanics/an-idealised-biphasic-poroelastic-finite-element-model-of-a-tibial-fracture

INTECH
open science | open minds